

Article

Carbon Emissions and Vegetation Dynamics: Assessing the Spatiotemporal Environmental Impacts of Hydropower Dams in the Lancang River Basin

Yu Liu ¹, Xiaomao Wang ^{1,2}, Gang Ma ^{1,3}, Wei Zhou ^{1,3,*} and Xiang Cheng ^{1,4,*}

¹ Water Engineering Science Research Institute, Wuhan University, Wuhan 430072, China; 2022186540010@whu.edu.cn (Y.L.); wangxiaomao@cjsjy.com.cn (X.W.); magang630@whu.edu.cn (G.M.)

² CISPDR Corporation, Changjiang Water Resources Commission of the Ministry of Water Resources, Wuhan 430014, China

³ State Key Laboratory of Water Resources Engineering and Management, Wuhan University, Wuhan 430072, China

⁴ China Antarctic Surveying and Mapping Research Center, Wuhan University, Wuhan 430072, China

* Correspondence: zw_mxx@whu.edu.cn (W.Z.); xiang.cheng@whu.edu.cn (X.C.)

Abstract: Recent decades in the Lancang River Basin have witnessed extensive construction of hydropower dams, profoundly impacting the local environment. Utilizing high-precision satellite data, we conducted a comprehensive analysis of vegetation cover and carbon emissions, integrating data-driven time series and spatial analysis models to capture both temporal and spatial dynamics. Our findings reveal that hydropower dam construction in the Lancang River Basin has significantly promoted vegetation restoration and growth, concurrently facilitating a reduction in regional carbon emissions. Employing deep learning models for time-series prediction, we observed a substantial increase in the sum of the local normalized difference vegetation index (NDVI) post-construction, with an average rise of from 16.15% to a maximum of 20.12% during the pivotal hydropower dams' operational phase. Between 2001 and 2020, the construction of hydropower dams in the basin corresponded to notable changes in ecological and carbon metrics. Specifically, vegetation cover expansion intensity (VCEI) reversed from a negative mean of -0.009 to a positive mean of 0.008. Additionally, the carbon emission intensity (CEI) around these dams drastically reduced, shifting from an average of 0.877 to 0.052. Importantly, the Global Moran's I for VCEI significantly increased from 0.288 pre-2016 to 0.679 post-2015, reflecting a stronger spatial autocorrelation in vegetation patterns. Accordingly, these findings illustrate the complex interplay between hydropower dams and environmental outcomes, underscoring the critical role of pivotal hydropower dam construction in ecological improvement. The research results have improved and complemented those of previous studies on the environmental impact of hydraulic engineering, providing valuable insights for the construction management and policy formulation of hydropower dams in other similar river basins around the world.



Citation: Liu, Y.; Wang, X.; Ma, G.; Zhou, W.; Cheng, X. Carbon Emissions and Vegetation Dynamics: Assessing the Spatiotemporal Environmental Impacts of Hydropower Dams in the Lancang River Basin. *Forests* **2024**, *15*, 872. <https://doi.org/10.3390/f15050872>

Academic Editor: Sheikh Adil Edrisi

Received: 4 April 2024

Revised: 13 May 2024

Accepted: 13 May 2024

Published: 17 May 2024

Keywords: Lancang River Basin; hydropower dams; data-driven time series; spatial analysis models; vegetation recovery; carbon mitigation



Copyright: © 2024 by the authors. Licensee MDPI, Basel, Switzerland. This article is an open access article distributed under the terms and conditions of the Creative Commons Attribution (CC BY) license (<https://creativecommons.org/licenses/by/4.0/>).

1. Introduction

The Lancang River Basin, traversing diverse ecological landscapes from the Tibetan Plateau to Southeast Asia, serves as a critical hub of environmental and socioeconomic vitality [1,2]. A notable change in energy engineering in the basin, primarily characterized by the construction of numerous hydropower dams, has been instituted to meet the escalating demand for clean energy [3]. Dam construction can alter the local climate by modifying land surface properties and water distribution, thereby influencing regional temperature and precipitation patterns, resulting in substantial environmental modifications [4–7].

At the dawn of the 21st century, the Chinese government launched a comprehensive initiative to harness the hydroelectric potential of the Lancang River Basin, spanning the Yunnan and Tibet provinces. This ambitious undertaking segmented the river into three distinct engineering zones with a total of 16 hydropower dams, including three pivotal hydropower dams for systematic engineering development.

However, several empirical studies have provided evidence that the hydropower infrastructure of the basin has spurred significant economic growth [8,9] but also caused damage to the environment [10,11]. This dual nature of dam construction boosts energy production while also disrupting ecosystems [12,13] and reducing carbon storage. For example, in their inquiry into sustainable development within the Lancang River Basin, Fan et al. found that the construction of dams has precipitated a reduction in both monsoonal floodwater volume and annual sediment discharge within China. As a consequence, this decline has facilitated the deterioration of reservoir water quality [14]. The use of NDVI analysis in a study by Yigzaw and Hossain further revealed a downward trend in vegetation health, with a mean annual NDVI decrease between 2000 and 2012 in multiple large dam cities in the US [15]. The research of Liu et al. on the NDVI within regions both upstream and downstream of the Danjiangkou reservoir from 1982 to 2018, revealed a substantial reduction in the NDVI downstream of the dam and within the proximate central city regions [16]. Li et al. used canonical correspondence analysis (CCA) to provide conclusive evidence that cascade dam construction developments have significantly exacerbated ecological damage within the basin. One of the most pronounced effects observed is the reduction in vegetation complexity and distribution [17]. The research of Long and Zhou indicates that although dam construction has increased local carbon storage in the long run, the development of hydropower facilities and the subsequent rise in reservoir water levels have led to a significant amount of land inundation. This dynamic has, in turn, precipitated a considerable loss of carbon storage within the reservoir areas [18].

In light of China's commitment to 'carbon neutrality' and its 'carbon peak' objectives [19], alongside stringent environmental protection laws that preclude compromising environmental integrity for economic development [20,21], the continued emphasis on dam construction in the Lancang River Basin presents an obvious paradox. This phenomenon raises critical questions about the congruence of such infrastructural developments with the China's environmental and carbon mitigation strategies.

Our research posits that the proliferation of hydropower dams in this region may not be antithetical to environmental conservation and carbon neutrality goals. We believe that, since the early 21st century, the hydropower dams in the Lancang River Basin appear to have contributed to not only regional economic advancement [22–24] but also to ecological benefits, including the rehabilitation and expansion of local vegetation, potentially acting as a significant factor in the reduction of carbon emissions. More importantly, the construction of hydropower dams in this region represents a critical shift towards renewable energy sources intended to support both national energy security and global sustainability targets, including those outlined in the United Nations Sustainable Development Goals (UNSDGs), such as Affordable and Clean Energy (Goal 7) and Climate Action (Goal 13).

Our study, therefore, aims to rigorously evaluate the environmental impacts of hydropower dam construction in the basin over this period. Our inquiry spans two decades from 2001 to 2020, a period marked by significant hydroelectric infrastructure development, including the completion and near-completion of hydropower dams. To validate our hypothesis, we conducted a robust evaluation of the hydropower dams of the Lancang River Basin. Our methodology integrated advanced spatial and time-series analytical models, supported by a comprehensive multivariate data approach. Utilizing a fusion of remote sensing satellite data, we meticulously analysed the spatiotemporal variation in vegetation coverage and carbon emissions.

We leveraged the predictive capabilities of the NeuralProphet model, which adeptly incorporates seasonal variations, to enhance the accuracy of NDVI index forecasts across the Lancang River Basin. By treating the pre-dam construction phase as a baseline, the

model adeptly projected potential vegetation cover trajectories in the absence of dam interventions. The subsequent juxtaposition of these projections against the actual post-construction vegetation dynamics revealed a distinct positive feedback loop, wherein dam construction bolstered vegetation health. Meanwhile, our analysis employed a spatiotemporal geographically weighted regression (GTWR) model, a sophisticated approach to unravelling the complex interplay of factors driving regional carbon emissions. Moreover, on the premise of introducing economic and demographic variables, through detailed analysis of the model's fitting coefficients, we were able to disaggregate and quantify the relative impacts of demographic, economic, and vegetation coverage variables on the carbon emission profile of the basin. Finally, we utilized Global Moran's I to examine the spatial clustering of VCEI, assessing the effects of dam construction on the spatial patterns of vegetation cover expansion.

Our findings highlight the pivotal role of hydropower dams in advancing regional environmental restoration and development, while complementing the findings of previous studies in the related fields of dam construction and environmental impact. As global energy demand escalates, this comprehensive evaluation underscores the transformative effects of dam construction on the Lancang River Basin and offers critical insights into the environmental implications of hydropower projects across comparable river systems worldwide. This analysis bolsters the development of hydropower and other renewable energy sources, contributing to the achievement of the UNSDGs.

2. Study Area

The Lancang River Basin spans approximately 167,400 square kilometers, with the main river extending over 2161 km, positioned in the southwestern region of China proximate to the border, and exhibits unique environmental characteristics of low population density and limited influence from official environmental policies due to inherent environmental constraints [25]. In contrast, the influence of natural environmental factors, particularly on local vegetation, assumes greater significance.

The basin's hydrology is predominantly influenced by precipitation, supplemented by groundwater and snowmelt inputs [26]. Climatic conditions in the basin vary significantly from the Tibetan stretch to the mid-lower Yunnan stretch. The Tibetan stretch is characterized by a temperate plateau climate with an average annual temperature of 10 °C and precipitation ranging from 400 to 800 mm. In the upper Yunnan reach, a subtropical climate prevails, with temperatures of 12–15 °C and precipitation between 1000 and 2500 mm, mainly in mountainous areas. The mid-lower Yunnan stretch experiences a subtropical to tropical climate, with temperatures of 15–22 °C and annual rainfall of 1000 to 3000 mm. The region is dominated by a monsoon climate, featuring a wet season from May to October and a dry season from November to April, with 85% of rainfall occurring in the wet season and 60% of that concentrated between June and August [27]. Recent climatological analyses reveal a pronounced warming trend in the Lancang River Basin, with temperatures rising by approximately 3 °C in recent years. This increase in temperature is concurrent with changes in precipitation patterns, characterized by a marked intensification during the monsoon period from June to October [28]. At the same time, the soil landscape in the basin is predominantly shaped by natural erosion processes [27].

Among the various factors shaping the environment, the construction of reservoirs stands out as a primary driver of environmental change. Reservoir construction directly alters environmental parameters such as precipitation patterns [29], temperature levels [30], and soil quality [31], which in turn affect vegetation dynamics. Considering the overarching influence of hydropower dams on the environmental dynamics of the Lancang River Basin, other factors affecting vegetation can be deemed relatively insignificant. Consequently, while acknowledging the complex interplay of various environmental elements, the direct impact of hydropower dams on vegetation warrants focused attention in environmental assessments.

Our research meticulously delineates the geographical scope to counties within the Lancang River Basin directly affected by hydropower dams and those in the periphery

impacted by these hydrological developments. As shown in Figure 1a, The study comprehensively covers 50 county-level regions, strategically segmented into nine counties in the Tibetan stretch, sixteen in the upper Yunnan stretch, and twenty-five in the mid-lower Yunnan stretch. Meanwhile, the identification of nine counties as primary dam sites (dam counties) is informed by administrative jurisdictional boundaries, considering that several hydropower dams straddle the interface of distinct regions. This delineation is instrumental to understanding the socioeconomic dynamics, as the fiscal revenues and operational maintenance of hydropower dams are closely tied to their administrative regions. In parallel, by focusing our research on specific administrative divisions, we can more effectively align with the policy needs of local governments, thereby ensuring that our findings exert a direct influence on policy formulation and environmental management. Additionally, the inherent geographical and socioeconomic uniformity within administrative regions facilitates a systematic analysis and understanding of the specific environmental impacts of dam construction.

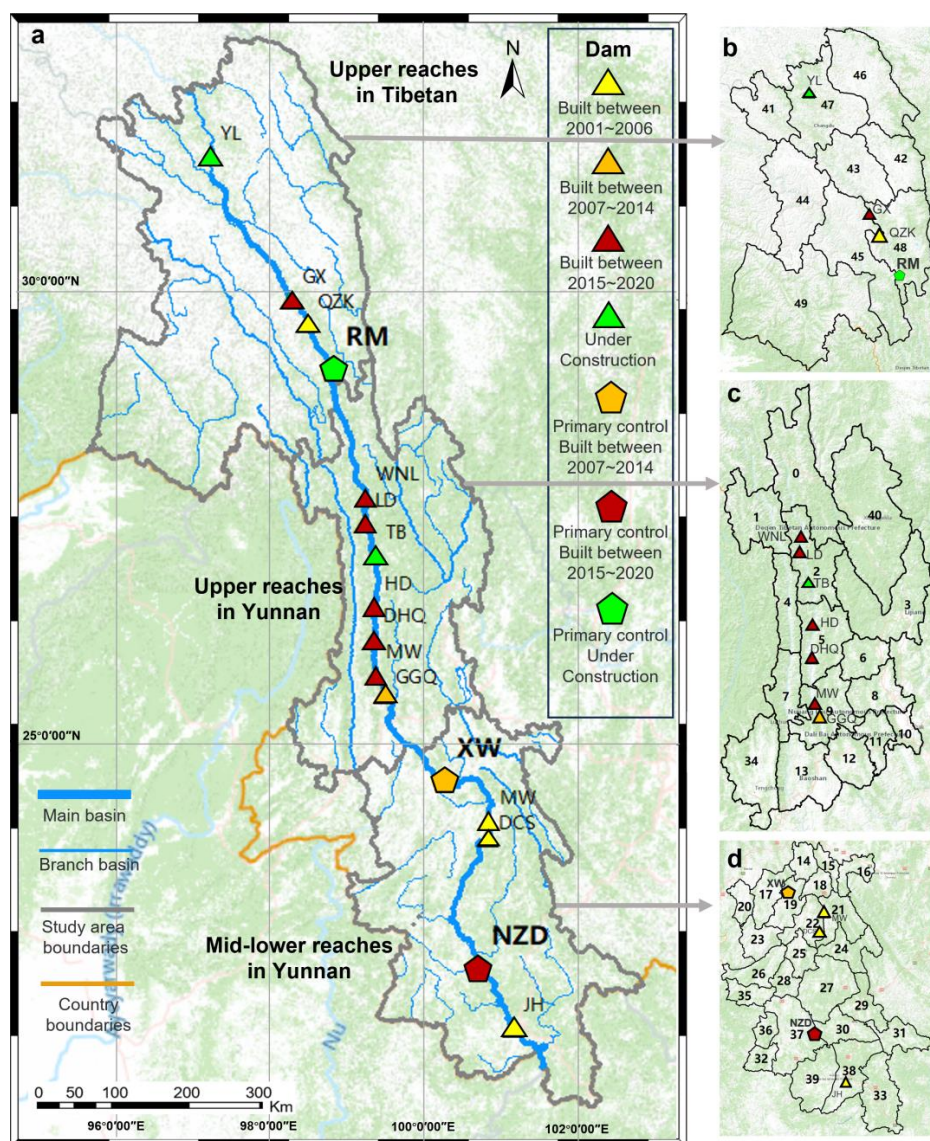


Figure 1. (a) The distribution of hydropower dams within the Lancang River Basin is depicted, where triangles represent auxiliary hydropower dams and pentagons denote the primary control hydropower dams. (b) In the Tibetan stretch, there are nine counties in total. (c) In the upper Yunnan stretch, there are 16 counties in total. (d) In the mid-lower Yunnan stretch of the basin, there are 25 counties in total.

Table 1 lists key information on dams in the Lancang River Basin. The Tibetan stretch is dedicated to the “One Reservoir, Eight-Level” scheme, featuring eight hydropower dams, inclusive of a pivotal dam (RuMei, RM), targeting a collective installed capacity of 6.38 million kilowatts. Descending to the upper Yunnan reach, the “One Reservoir, Seven-Level” project is designed to achieve an 8.83 million kilowatt installed capacity, inclusive of a pivotal dam (GuShui, GS), with five hydropower dams currently functional. Further downstream, the mid-lower Yunnan stretch is progressing through the “Two Reservoirs, Eight-Level” blueprint, aiming for a 16.52-million-kilowatt cumulative capacity. The XiaoWan (XW) and NuoZhaDu (NZD) hydropower dams, completed in 2011 and 2014, respectively, are pivotal dams in the region.

Table 1. Dam construction in the Lancang River Basin.

Dam	Engineering Time	Storage	Dam	Engineering Time	Storage
Ce Ge	Under design	/	Huang Deng	2008–2019	15.00 BCM
Yu Long	2015–Now	19.70 BCM	Da HuaQiao	2010–2019	3.15 BCM
Ka Gong	Under design	/	Miao Wei	2012–2017	6.60 BCM
Ban Da	2019–2021	13.19 BCM	Gong Guoqiao	2009–2012	3.15 BCM
Ru Mei	2013–Now	24.33 BCM	XiaoWan (Pivotal dam)	2002–2010	150.00 BCM
Bang Duo	Under design	/	Man Wan	1987–1993	9.20 BCM
Gu Xue	2012–2021	26.84 BCM	Da ChaoShan	1992–2003	9.40 BCM
QuZiKa	1982–1987	405.00 BCM	Nuo ZhaDu (Pivotal dam)	2012–2014	237.03 BCM
Gu Shui	Under design	/	Jin Hong	2003–2008	11.39 BCM
Wu NongLong	2010–2021	2.84 BCM	Gan LanBa	Under design	/
LiDi	2009–2019	0.75 BCM	Men Song	Under design	/
Tuo Ba	2018–Now	10.39 BCM			

The BCM unit in the table is Billion Cubic Meters.

3. Data and Methods

3.1. Source of Data

All data time periods used in our study were from 2001 to 2020. We utilized ArcPy together with the GDAL open-source library for transforming raster spatial data. Initially, this approach allowed us to correct various remote sensing raster datasets and perform a primary batch-cropping based on vector data of the study region. We then applied ArcPy’s raster calculation tools to derive total raster values for the area, which facilitated the analysis of trends in statistical elements from 2001 to 2020. Following this, we conducted a secondary batch-cropping tailored to the vector outlines of individual counties.

1. NDVI Data: We utilized MODIS satellite NDVI data obtained from the Earth Science Data and Information System (ESDIS) project under NASA’s Earthdata platform (<http://search.earthdata.nasa.gov>, accessed on 20 September 2023). The dataset spans from 2001 to 2020, with NDVI values updated every 16 days. The spatial resolution of these data is $0.5 \text{ km} \times 0.5 \text{ km}$. As outlined in Table 2, we categorized the NDVI index into five distinct classes for comprehensive analysis.
2. Carbon Emission Data: We used the Open-source Data Inventory for Anthropogenic CO₂ (ODIAC) dataset, specifically the ODIAC2022 version, produced and released by the National Institute for Environmental Studies, Japan. The dataset can be accessed at the ODIAC Fossil Fuel Emission Dataset (https://db.cger.nies.go.jp/dataset/ODIAC/DL_odiac2022.html, accessed on 20 September 2023) and offers a resolution of $1 \text{ km} \times 1 \text{ km}$, providing a detailed account of global fossil fuel combustion-related CO₂ emissions.

Table 2. NDVI classification.

Classification	Vegetation Coverage	Range of Value	Vegetation Type
Category 5	High	0.8 > AND ≤ 0.2	Dense forests, High-density jungle.
Category 4	Medium to high	0.6 > AND ≤ 0.8	robust shrublands, General jungle.
Category 3	median	0.4 > AND ≤ 0.6	shrublands, harvested fields.
Category 2	Medium low	0.2 > AND ≤ 0.4	Mixed vegetation, grasslands. Agricultural land
Category 1	Low	0.0 > AND ≤ 0.2	Sparse vegetation, overgrazed lands.

3. Nighttime Light Data: We utilized processed NPP-VIIRS-like nighttime light data, referencing the methodological approach of Chen et al. [32]. This study rectified and aligned NPP-VIIRS with DMSP-OLS light data. The publication provided a continuous global light dataset from 2000 to 2018, using a computational method which we applied to derive light data for 2019 and 2020. The data resolution is $1 \text{ km} \times 1 \text{ km}$. In this study, we use lighting data to evaluate and replace local gross domestic product (GDP) [33].
4. Population Data: Our population data were sourced from the WorldPop global population dataset, an integration of adjusted data from Afripop, AsiaPop, and AmeriPop, compiled by the University of Southampton. The link is the WorldPop (<https://hub.worldpop.org/project/categories?id=18>, accessed on 25 October 2023) Project and offers a spatial resolution of $1 \text{ km} \times 1 \text{ km}$.
5. Land Use Data: We utilized the land use data for China segmented at $30 \text{ m} \times 30 \text{ m}$ data resolution [34]. This work involved the creation of an annual Chinese Land Cover Dataset (CLCD) based on Landsat imagery on the Google Earth Engine (GEE) platform. The dataset encompasses annual land cover classifications for China from 1990 to 2019 and documents the dynamic changes in these classifications over time. At present, the author has expanded the data range to 1985 to 2022.
6. Dam Information: We used the Global Georeferenced Database of Dams (GOODD) and the Future Hydropower Reservoirs and Dams (FHReD) database. GOODD is a comprehensive repository encompassing the geospatial coordinates of all hydropower dams visible on Google Earth satellite imagery, currently documenting 38,660 hydropower dams globally. FHReD, on the other hand, provides detailed mapping of about 3700 hydropower dams that are either under construction or in the advanced stages of planning.

3.2. NeuralProphet Prediction Model Based on Parameter Optimization

NeuralProphet (NP) represents a sophisticated evolution of the widely recognized Prophet model, harnessing the capabilities of machine learning for predictive analysis. As an enhancement of its predecessor, NP integrates neural network algorithms to capture more complex patterns within time-series data [35]. This advanced modeling approach is adept at adapting to nonlinear trends in time-series data, making it particularly effective for handling vegetation data characterized by strong seasonal fluctuations [36,37]. The implementation of NP allows for a nuanced understanding of temporal patterns, providing an innovative tool for analyzing and forecasting environmental data with high variability and intricate seasonal dynamics.

In our research, we have advanced the capabilities of the NP model by incorporating a random search methodology for the optimization of model parameters. This refined approach to NP utilizes an adaptive parameter optimization strategy, involving the careful definition of a hyperparameter space and the establishment of logical parameter range

boundaries. For example, the learning rate was set within a spectrum of 0.001 to 0.1, while the model lag length varied from 10 to 365 in increments of 10. Additionally, the range for model hidden layers was established at between 10 and 50, with increments of 10, and the batch size was configured to span from 32 to 256.

To rigorously evaluate the model's efficacy, we employed mean squared error (MSE) and root mean squared error (RMSE) as our primary performance metrics, alongside a four-fold cross-validation method to bolster the model's generalizability. A meticulous random search was conducted across varying parameter combinations, guiding the training and evaluation of the NP model to ascertain the most effective parameter set within the defined search domain. We explored multiple search ranges for optimal model fitting; currently, for each set of hyperparameters, 15 distinct search ranges have been tested. This quasi-grid search optimization technique, despite its intensive computational demands, ensures the exhaustive and robust parameter optimization of the NP model, enhancing the precision and reliability of our time-series analysis. Our study delineates the vegetation cover changes attributable to dam construction through the following steps:

1. We divided the dataset into two segments using the dam's completion date as the demarcation point: pre-completion data for model training and post-completion data for predictive analysis.
2. The optimal parameters for the vegetation cover change prediction model were derived from the training set, which represents the period before the dam's completion. During this phase, the dam's hydroelectric facilities were either not operational or only partially functional, thereby reflecting vegetation cover changes unaffected by the dam.
3. Utilizing this model, we predicted vegetation cover changes for the period post-dam completion. This data-driven approach enabled the projection of vegetation trends under a hypothetical scenario where the dam was not constructed.
4. By comparing the model-predicted vegetation trends with actual observed changes, we quantified the impact of dam construction on local vegetation. The difference between these two datasets provides a measure of the dam's influence.

3.3. Geographically and Temporally Weighted Regression (GTWR)

The GTWR model represents a sophisticated statistical analysis methodology that synergizes spatial and temporal factors [38]. Meanwhile, this model amalgamates the principles of geographically weighted regression (GWR) with those of time-series analysis [39]. GTWR is particularly designed to analyze how data evolve over time and exhibit spatial variability, thereby acknowledging spatial heterogeneity while incorporating the temporal dimension [39]. Therefore, this approach is instrumental in uncovering localized the spatial and temporal characteristics of datasets [40].

In the GTWR model, each county within our study is represented by its centroid coordinates, allowing a single sample point to represent each county area. The fundamental formula for GTWR is as follows:

$$Y_i = \beta_0(\mu_i, v_i, t_i) + \sum_k \beta_k(\mu_i, v_i, t_i) X_{it} + d_i$$

where (μ_i, v_i, t_i) denote the spatiotemporal coordinates of i^{th} county. μ_i, v_i , and t_i are the longitude, latitude, and time, respectively. $\beta_0(\mu_i, v_i, t_i)$ is the regression constant for the i^{th} sample point, while $\beta_k(\mu_i, v_i, t_i)$ denotes the K^{th} regression parameter. X_{it} is the value of the K^{th} independent variable at point i , and d_i is the residual error. The estimation of $\beta_k(\mu_0, v_0, t_0)$ is conducted using the following formula:

$$\hat{\beta}(\mu_i, v_i, t_i) X_{it} = \left[X^T W(\mu_i, v_i, t_i) X \right]^{-1} X^T W(\mu_i, v_i, t_i) Y$$

$\hat{\beta}(\mu_i, v_i, t_i)$ represents the estimated value of $\beta_k(\mu_i, v_i, t_i)$, X is the matrix of independent variables, and Y is the matrix of dependent variables. $W(\mu_i, v_i, t_i)$ is the spatiotemporal

weight matrix based on Euclidean distances and the Gaussian kernel function. The calculation formula for the spatiotemporal weight matrix is as follows:

$$W(\mu_i, v_i, t_i) = W^{time}(\mu_i, v_i, t_i) \times W^{space}(\mu_i, v_i, t_i)$$

$$W^{time}(\mu_i, v_i, t_i) = \exp\left(-\frac{d_{ij}^2}{h_{time}^2}\right)$$

$$W^{space}(\mu_i, v_i, t_i) = \exp\left(-\frac{D_{ij}^2}{h_{space}^2}\right)$$

$$d_{ij} = \sqrt{(t_i - t_j)^2}$$

$$D_{ij} = \sqrt{(\mu_i - \mu_j)^2 + (v_i - v_j)^2}$$

In this formula, $W^{time}(\mu_i, v_i, t_i)$ and $W^{space}(\mu_i, v_i, t_i)$ represent the time and space weight matrices, respectively. h_{time} and h_{space} are the bandwidths for time and space weights, while d_{ij} and D_{ij} denote the temporal and spatial distances between sample point i and point j .

We employed the GTWR model to dissect the complex array of factors contributing to total carbon emissions in various counties. Within our model framework, we identified county-level total carbon emissions as the dependent variable and integrated key predictors including total GDP, population, and NDVI values for each sample point as independent variables. To ensure analytical consistency and comparability, a thorough standardization process was applied to all variables, followed by rigorous multicollinearity testing, a prerequisite step before incorporating these variables into the GTWR model. Our analysis was segmented into three time intervals: 2001–2006, 2007–2014 (which marks the phase of concentrated dam construction), and 2015–2020. By scrutinizing the coefficients' magnitude for each interval, we could quantify the relative impact of each driver on total carbon emissions. Moreover, comparing the variations in coefficients across these time periods enabled us to unravel the dynamic shifts in carbon emission drivers, thereby illuminating the evolving temporal patterns and trends that shape the landscape of carbon emission determinants.

3.4. Spatial Correlation Analysis of Expansion Intensity

We assessed the average intensities of vegetation cover and carbon emission expansion across three distinct time periods (the GTWR research period) within the Lancang River Basin counties. To mitigate the influence of seasonal variability on vegetation cover growth and carbon emissions, we utilized the annual cumulative NDVI indices and total carbon emissions for our calculations. This approach allowed us to quantify the relative changes in the vegetation cover index and total carbon emissions within each specific timeframe.

The formulas for calculating the average intensities of vegetation expansion and carbon emission expansion are as follows:

$$\Delta T = T_{End_year} - T_{Sta_year}$$

$$U_i = \frac{\sum_{i=1}^{\Delta T} U_{Sta_year+i} - U_{Sta_year}}{\Delta T \times U_{Sta_year}} \times 100\%$$

where T_{End_year} and T_{Sta_year} represent the calculation data at the beginning and end of each period, and ΔT is the duration of the calculation period expressed in years. U_i signifies the average intensity of calculation data over the defined time period. U_{Sta_year} corresponds to the calculation data at the beginning of the calculation period.

3.5. Global Moran Index (Global Moran's I)

We use the Global Moran Index to measure the spatial clustering of vegetation cover expansion intensity (VCEI) and diminished carbon emission intensity (CEI). Moran's I, a global measure of spatial autocorrelation, serves as a fundamental tool in analyzing spatial patterns and similarities in variable distributions. Introduced by Patrick Moran in 1950, this statistical method evaluates whether spatial data exhibit randomness or discernible patterns such as clustering, dispersion, or regular spatial distribution [41]. The formula for calculating Global Moran's I is as follows:

$$I = \frac{n}{S_o} \times \frac{\sum_{i=1}^n \sum_{j=1}^n w_{i,j} z_i z_j}{\sum_{i=1}^n z_i^2}$$

$$S_o = \sum_{i=1}^n \sum_{j=1}^n w_{i,j} z_i z_j$$

where z_i is the deviation between the attribute of element i and its average value ($x_i - \bar{X}$), $w_{i,j}$ is the spatial weight between elements i and j , n represents the total number of elements, and S_o is the aggregation of all spatial weights.

Global Moran's I, as measured by the Pearson correlation coefficient values, reflects the degree of spatial clustering. Values of I approaching +1 or -1 indicate strong spatial clustering, with +1 suggesting that entities share similar attributes and -1 indicating that entities are dissimilar. Conversely, values of I close to 0 signify weak spatial clustering.

4. Results

4.1. Changes in Total Vegetation Coverage in the Lancang River Basin

4.1.1. Comparison of NDVI Vegetation Cover Classification

We classified the NDVI index into five categories of vegetation cover, as shown in Table 2. We distinguished between dam counties and non-dam counties, calculating the proportion of each NDVI category in both types of counties. As shown in Figure 2a,b, after comparing the vegetation cover in dam and non-dam counties, we found that the first category of vegetation cover in dam counties was significantly lower than that in non-dam counties, while the second and third categories were noticeably higher. The decrease in the first category and increase in the second and third categories of vegetation cover suggest a gradual transition from wasteland to grassland and shrubland in the area, indicating an increase in vegetation restoration efforts. The fourth category of vegetation cover in dam counties was lower than in non-dam counties. However, between 2001 and 2020, the proportion of the fourth category of vegetation cover gradually increased at a faster rate than in non-dam counties. After the completion of numerous hydroelectric dams in 2015, the fourth category of vegetation cover in dam and non-dam counties became nearly identical each year. The vegetation restoration efforts in dam counties outpaced those in non-dam counties. As illustrated in Figure 2c, when comparing the average NDVI values per square kilometer between dam counties and non-dam counties over the years, we observed that from 2001 to 2020, dam counties consistently exhibited higher NDVI values than non-dam counties. This indicates that the vegetation cover in dam counties is superior to that in non-dam counties.

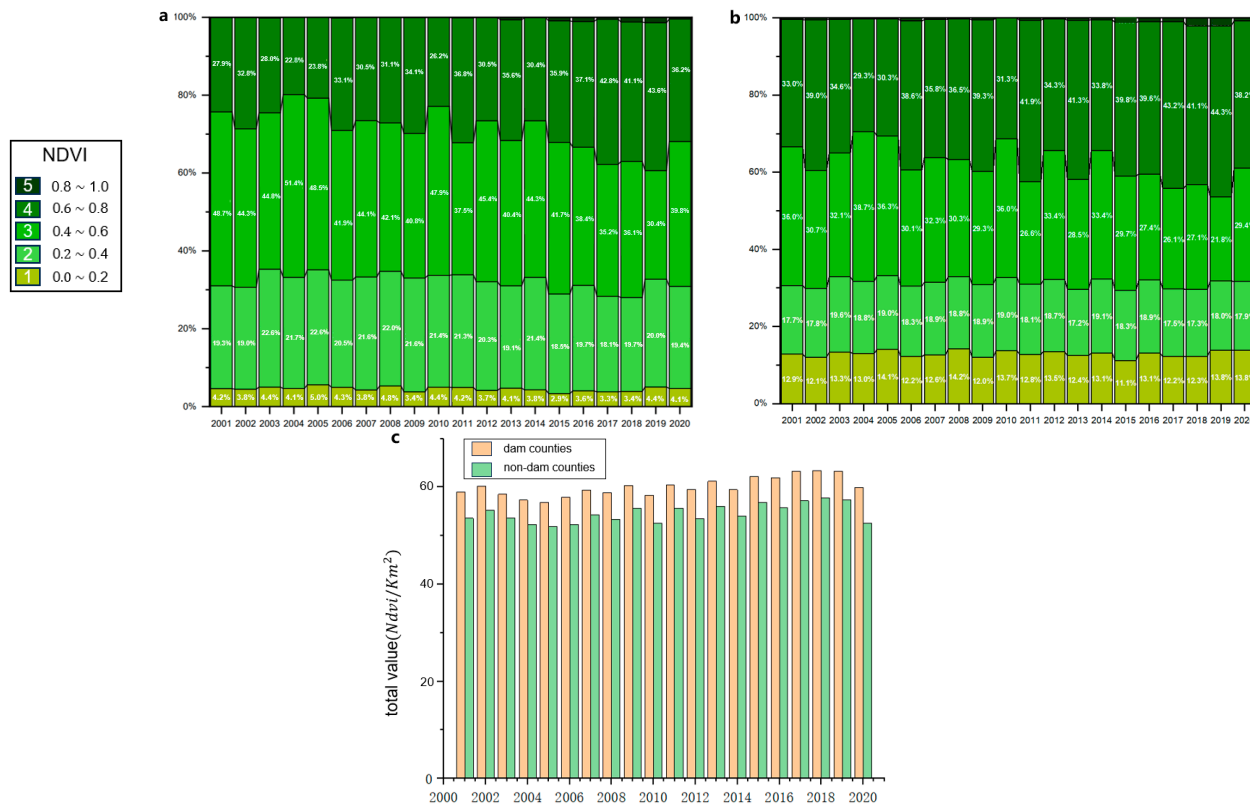


Figure 2. (a) Comparison of NDVI classification in dam counties. (b) Comparison of NDVI classification in non-dam counties. (c) Comparison of the average total NDVI values per square kilometer between dam and non-dam counties in the basin.

4.1.2. Quantitative Analysis of the Impact of Dam Construction on Vegetation Cover

In the construction of the cascade dam system within the Lancang River Basin, both pivotal and auxiliary hydropower dams are included. Due to their massive scale, pivotal hydropower dams have a more significant and widespread environmental impact. These pivotal hydropower dams are often prioritized as regional key hydraulic projects, attracting substantial construction investments and consequently exerting profound influences on local economies and policy formulations [42].

Therefore, our study primarily focuses on the pivotal hydropower dams in the basin. Among these, there are three pivotal hydropower dams: the RM, XW, and NZD. Given that the RM dam is not yet fully operational, and the XW dam only commenced full-scale power generation in 2010, the data-span from 2001 to 2010 is too limited for effective model training, adversely affecting the model's accuracy. In contrast, the NZD dam was completed in 2014, allowing for the utilization of data from 2001 to 2014 as the training set, which constitutes 70% of the total data volume. Therefore, we have selected the NZD dam as the focus of our study. Utilizing the adaptive parameter optimization capabilities of the NP model, we perform a quantitative analysis of the impact on vegetation cover caused by the construction of the NZD dam.

As illustrated in Figure 3, the NZD dam is located at the junction of counties No. 37 and No. 30, which are directly impacted by the dam. In accordance with the First Law of Geography, which states that everything is related and things closer together are more closely related, we selected counties No. 27, No. 28, No. 32, No. 35, No. 36, and No. 39 as our model training dataset to minimize the influence of other geographical factors. These counties are not directly affected by the NZD dam construction. To align with the operational period of the NZD dam, we used data from 2001 to 2014 for model training, with the data from 2010 to 2014 serving as the validation set, and data from 2014 to 2020 as the prediction set. The training results, as shown in Figure 3, reveal that the model

accurately captures the cyclical trends in vegetation cover. The model's fitted curves exhibit high congruence with the actual vegetation cycle, demonstrating the model's efficacy in predicting periodic vegetation changes.

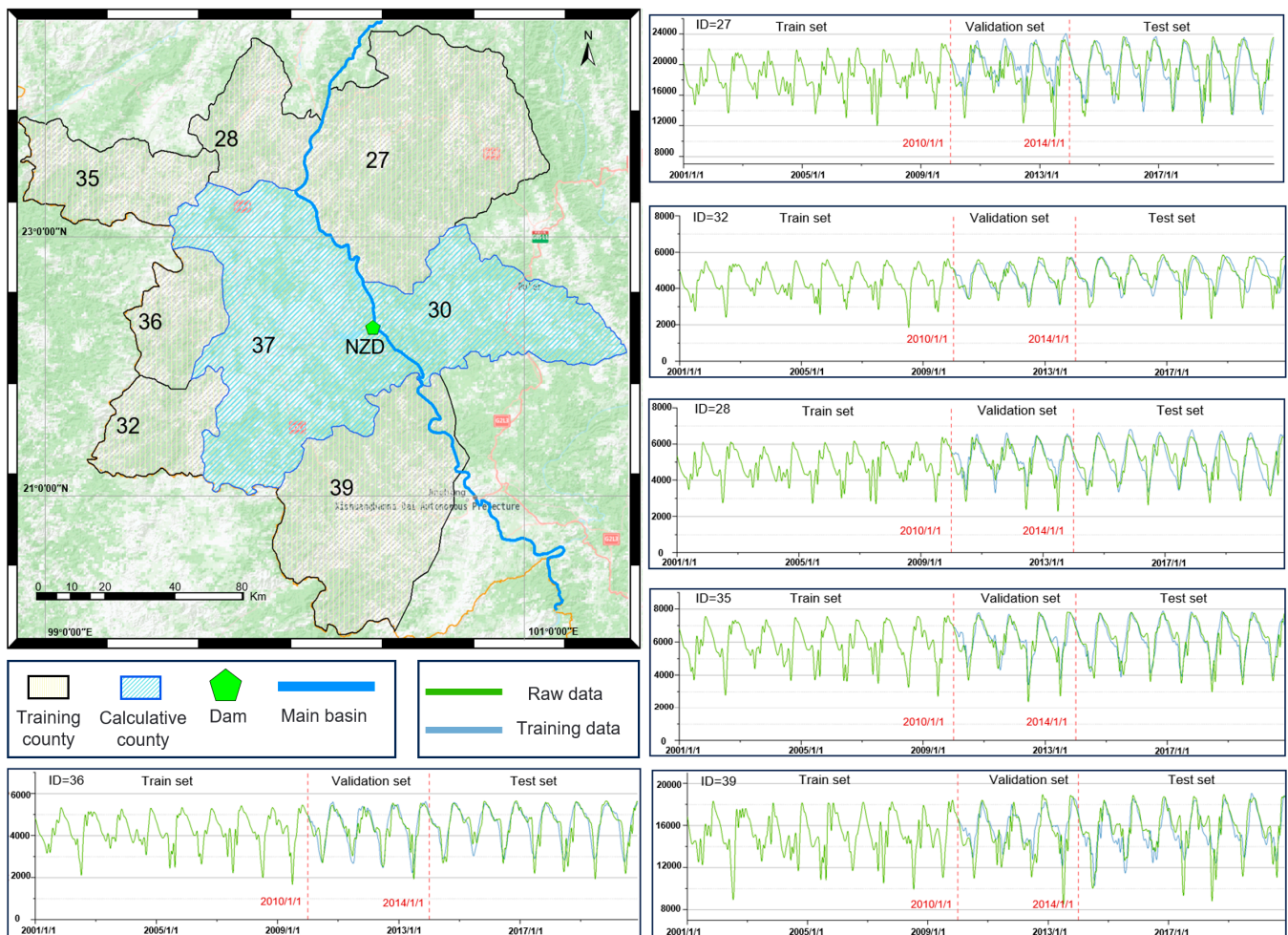


Figure 3. The areas highlighted in yellow represent the training counties, which are not influenced by dam construction. The time-series prediction model was trained using the dataset to produce forecast curves, where the green line segment represents actual data, and the blue line segment represents predicted data.

The model prediction error results are shown in Figure 4a. Comparing the model predictions with the actual values, we found that county No. 27 had the best model fit, with an annual average error rate of 7.79%. In contrast, county No. 32 had the poorest fit, with an annual average error rate of 12.44%. The average annual error rate for all training counties was 10.96%. As illustrated in Figure 4b, which compares the error between the model's validation set and the training set, except for county No. 32, the error rates for the validation and test sets in the other counties were similar. This indicates that the model has good generalization capabilities on unseen data. Across multiple counties, the model demonstrated similar and high predictive accuracy, reflecting its robustness.



Figure 4. (a) The error statistics for the training set of the time-series prediction model. (b) Comparison of the errors between the validation set and the training set. As indicated in the legend, we divided the model error data into ten categories, calculating the average annual error for each county (all errors in the figure are taken as absolute values).

However, while the vegetation data generally fluctuate annually, there is variability within each cycle in individual years, including some extreme values. Due to its time-series characteristics, the model was unable to predict these extreme values within the vegetation cycles. Therefore, the overall model prediction error was relatively high in 2018. As observed in Figure 3, the vegetation cover change curve for the training counties in 2018 had extreme values, which impacted the model's training accuracy. Combining the results from Figures 3 and 4, although the within-cycle variability slightly reduced the model's training accuracy, the model exhibited excellent predictive capabilities for vegetation cover data with high periodicity over larger time scales. The predictions closely mirrored the data's cyclicity, with low error rates between the predicted and actual values.

For the target counties No. 30 and No. 37, we utilized the period from 2001 to 2014, before the NZD dam became fully operational, as our training set, and the years from 2014 to 2020 as our prediction set. During the training period, as the dam was not yet operational, its impact on vegetation was minimal. Therefore, this period can be approximated as showing a natural growth state of vegetation without dam influence.

By using these data as the training set, the model developed can effectively predict the vegetation growth in the region from 2014 to 2020 under a scenario without the dam's influence. By comparing the model's predictions with the actual data from 2014 to 2020, we can quantitatively assess the impact of dam construction on local vegetation cover.

As shown in Figure 5, given that we selected vegetation cover data at 16-day intervals for area calculation, we adopted a limited approach, dividing the area into 16-day segments. By calculating the difference between the actual data and the calculated results, and summing them up, we approximated the area values to represent the increase in local NDVI. For county No. 30, the area of the real area contained in the green line segment is 160,8701.67 and the area of the yellow region is calculated to be 138,770.33 between the green and blue lines. For county No. 37, the real area is 324,8267.42 and the area of the yellow region is 201,232.03.

Considering the error comparison in Figure 4b, where the error in the validation set is approximately equal to that in the prediction set, we adjusted the prediction results by subtracting the error impact to approximate the actual values. The error for the validation set in county No. 30 is -9.76% , and for county No. 37 it is -5.22% . Further correction calculations reveal that the adjusted area of the yellow region for county No. 30 is 269,478.51, and for county No. 37 it is 352,396.49. Consequently, we conclude that due to the construction of the NZD dam, the total increase in the vegetation cover index for county No. 30 is 20.12%, with a specific NDVI total value increase of 269,478.51. For county No. 37, the total increase is 12.17%, with a specific NDVI total value increase of 352,396.49. The average growth rate in both regions is 16.15%. According to the calculation results, the vegetation coverage of the two areas affected by the NZD dam has significantly improved.

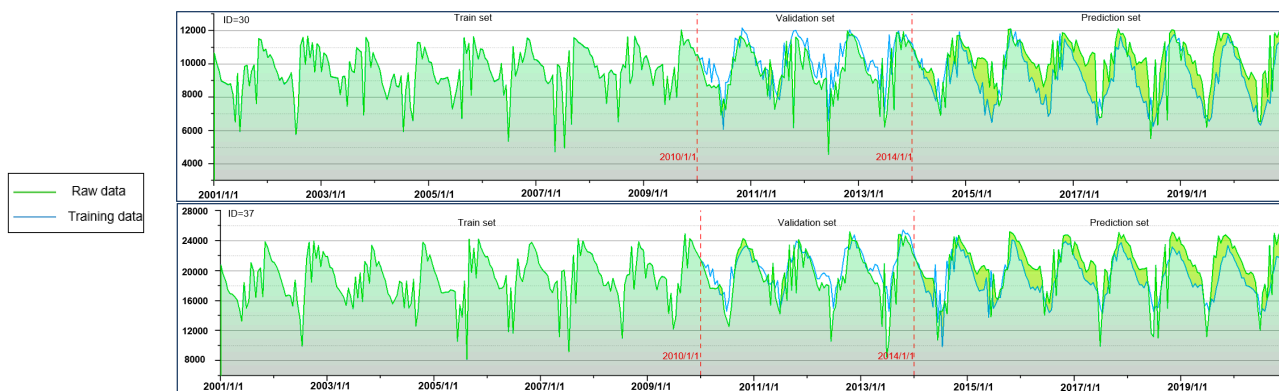


Figure 5. Results of the application of the target county time-series prediction model. The training results are depicted with the green line segment representing actual data and the blue line segment indicating predicted data. The yellow area, illustrating the difference between the green and blue lines, represents the impact of the NZD dam construction on counties No. 30 and No. 37. (Where the y axis represents the total NDVI in the target area, and the x axis represents the time).

4.2. Analysis of the Driving Mechanism of Total Carbon Emissions

We utilized the GTWR model, integrating satellite-derived nocturnal lighting data as a surrogate for local GDP. Additionally, total population size and a cumulative index of normalized vegetation cover were incorporated as explanatory variables. Initially, a standardization process was applied to all explanatory variables to ensure uniformity. The coefficients of these variables within the model were then used to quantify their respective impacts on regional carbon emissions. To address potential issues of spurious regression, a rigorous multicollinearity assessment was conducted for all explanatory variables. Table 3 presents the GTWR regression results, highlighting high model fitting across three distinct time periods, with Pearson correlation coefficients consistently exceeding 0.9.

Table 3. Related parameters of GTWR.

Year	Bandwidth	Residual Squares	Sigma	AICc	R ²	Adjusted R ²
2001–2006	0.11	0.16	0.02	-1330.95	0.94	0.94
2007–2014	0.11	0.49	0.04	-1441.96	0.96	0.96
2015–2020	0.11	0.37	0.03	-1068.39	0.97	0.97

Based on the spatiotemporal distribution of regression coefficients for the driving factors of total carbon emissions in the Lancang River Basin, the primary driving forces are determined by the extent of each factor's impact on carbon emissions in different counties (i.e., the comparison of the absolute values of regression coefficients across different periods). The influence of various drivers on the total carbon emissions of each county shows spatial heterogeneity over time.

By comparing the spatial changes in vegetation, we found that the overall vegetation cover has a minor and fluctuating impact on the region's total carbon emissions. As illustrated in Figure 6(a1), from 2001 to 2006, the contribution of total vegetation cover to high-value areas in carbon emissions shows a distinct division across the study area, with coefficient values progressively increasing from the Tibetan stretch to the mid-lower Yunnan stretch. Figure 6(a2) shows that during 2007–2014, the high-value areas positively influenced by total vegetation cover shifted in the upper Yunnan stretch, indicating that vegetation cover in this region promotes local carbon emissions. The high negative value areas were mainly concentrated in the Tibetan stretch counties. Figure 6(a3), covering the period from 2015 to 2020, shows that the high positive value areas influenced by total vegetation cover were located in the upper Yunnan stretch, while the high negative value areas were mostly along the Chinese border, with significant expansion in the mid-lower Yunnan stretch, particularly in counties No. 31, No. 32, No. 33, No. 38, and No. 39.

By comparing the spatial changes of GDP, we found that the influence of total regional GDP on carbon emissions remained consistently high throughout the study period, with a stable spatial distribution across all three periods. As depicted in Figure 6(b1), during the period from 2001 to 2006, the coefficient values for GDP showed a stepwise increase from the Tibetan stretch to the mid-lower Yunnan stretch, with high positive value areas mainly concentrated in the mid-lower Yunnan stretch. Figure 6(b2,b3) demonstrates that from 2007 to 2020, these high positive value areas continued to be focused in the mid-lower Yunnan stretch, gradually extending towards the upper Yunnan stretch.

By comparing the spatial changes of population, we found that the impact of regional population totals on carbon emissions showed more variability. As shown in Figure 6(c1), from 2001 to 2006, the high positive value areas for the population's impact on total carbon emissions were mainly concentrated in the Tibetan stretch and the upper Yunnan stretch. Figure 6(c2) reveals that between 2007 and 2014, the high value areas in the mid-lower Yunnan stretch gradually converged towards the upper area, with an increase in the number of low-value counties in the mid-lower stretch. As illustrated in Figure 6(c3), for the period from 2015 to 2020, the high negative value areas for population impact were primarily located in the Tibetan stretch, indicating a negative influence of population totals on carbon emissions in this region. Meanwhile, during the entire study period from 2001 to 2020, the upper Yunnan stretch consistently exhibited high positive value areas for population impact, suggesting that the total population in this region contributed to an increase in carbon emissions.

Figure 6d displays the distribution of coefficient changes for each explanatory variable across three time periods. By comparing the distributions of these three variables, it becomes apparent that over the years the impact of the total vegetation cover on carbon emissions has been less than that of GDP and population. However, from 2015 to 2020, when most hydropower dams began operation, the mitigating effect of vegetation cover on total carbon emissions gradually increased. The influence of GDP on total carbon emissions has consistently been at a higher level across the entire study area, with high-GDP regions often associated with higher total carbon emissions. The impact of GDP on carbon emissions significantly intensified from the 2001–2006 period to the 2007–2014 period, remaining at a high level.

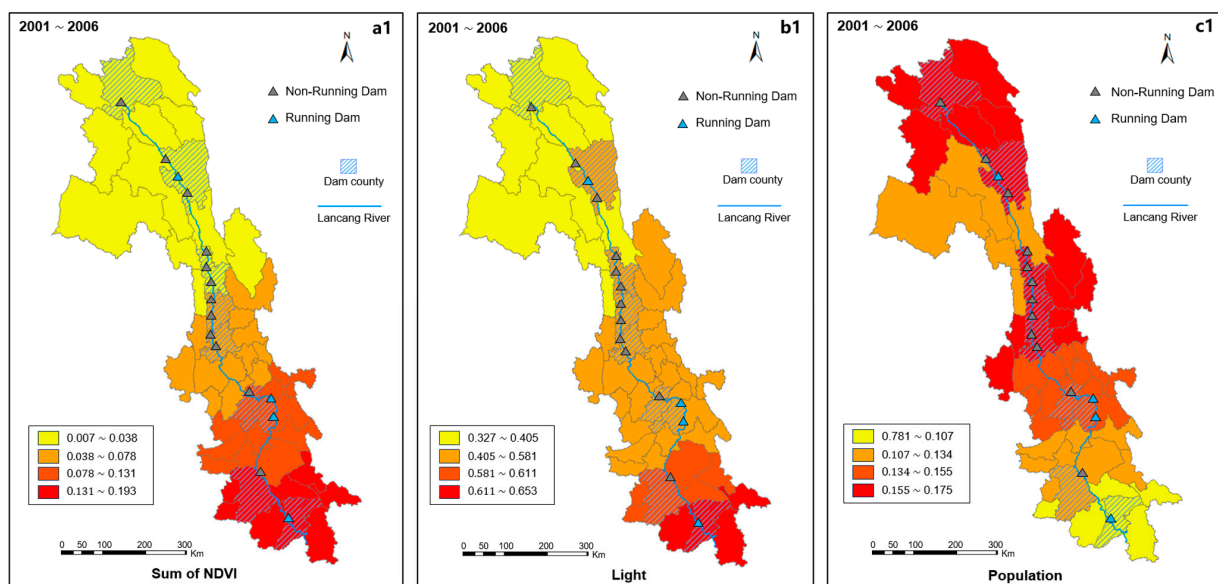


Figure 6. Cont.

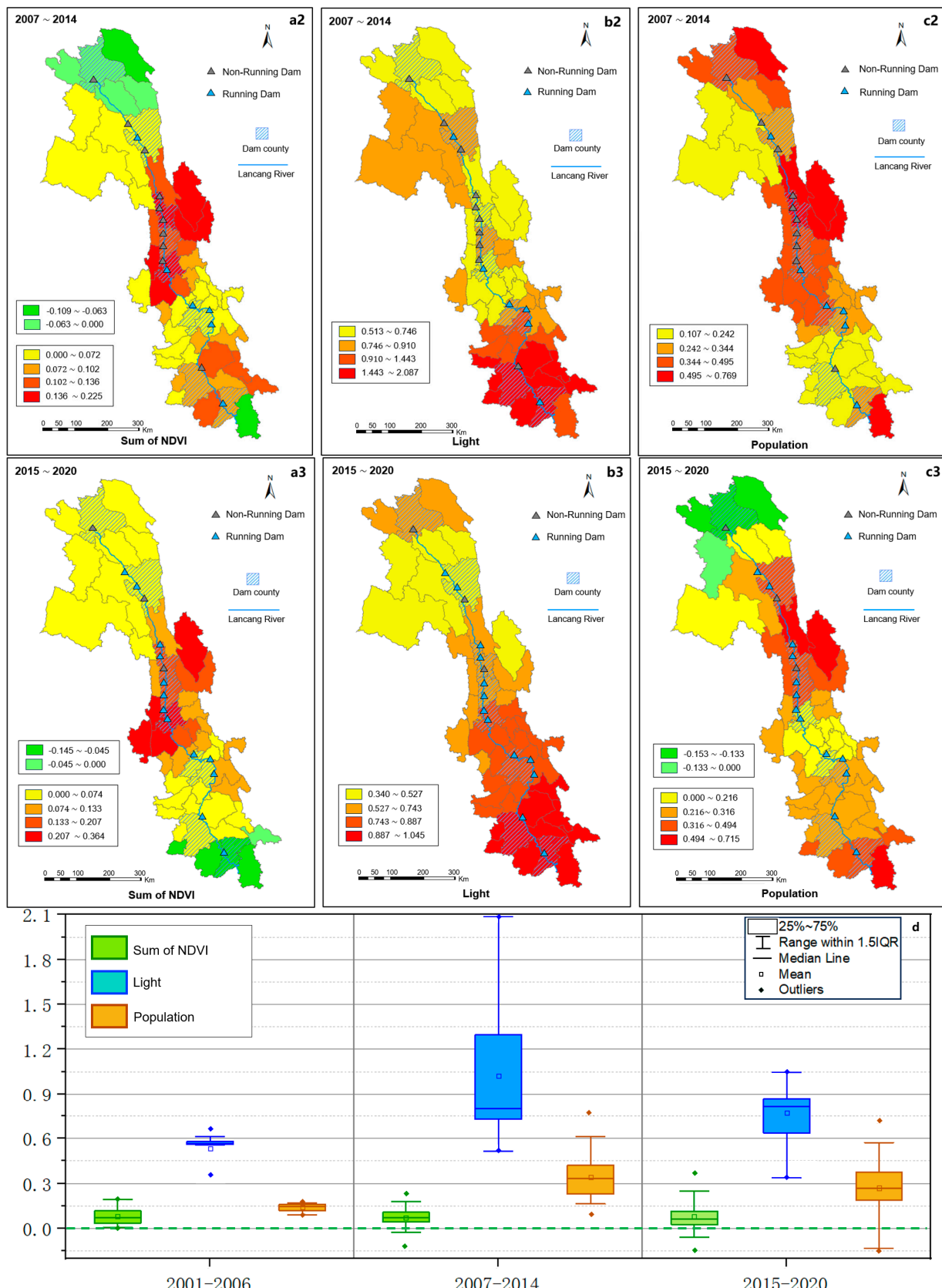


Figure 6. (a1–a3) Annual spatial distribution of NDVI regression coefficients in the GTWR model. (b1–b3) Annual spatial distribution of light regression coefficients in the GTWR model. (c1–c3) Annual spatial distribution of population regression coefficients in the GTWR model. (d) Distribution of annual coefficient changes for each explanatory variable.

4.3. Spatial Analysis of Vegetation Cover Expansion and Carbon Emission Intensity

We used the Global Moran Index to measure spatial clustering. In our spatial cluster analysis of vegetation cover expansion intensity (VCEI) and carbon emissions intensity (CEI) in the Lancang River Basin, we found a clear spatial clustering in VCEI. However, CEI, influenced by multiple factors, did not exhibit a pronounced spatial clustering pattern.

As indicated in Table 4, the Global Moran Index for VCEI from 2001 to 2020 was consistently positive and significant at the 5% level. Global Moran's I exhibited a stepwise increasing trend, indicating that during the three periods of dams in the basin the degree of spatial clustering in VCEI within the basin is continuously intensifying, with a pronounced trend towards concentrated distribution.

Table 4. Global Spatial Autocorrelation of VCEI.

Year	Moran's I	Z	P
2001 → 2006	0.288	3.473	0.001
2007 → 2014	0.560	6.296	0.001
2015 → 2020	0.679	7.998	0.001

As shown in Figure 7a–c, during 2001 to 2020, the VCEI in the basin showed a continual growth trend, characterized by significant spatial clustering and alternation effects. From 2001 to 2006, areas with positive expansion intensity were primarily concentrated in the mid-lower Yunnan stretch. In contrast, the upper Yunnan stretch and the Tibetan stretch exhibited negative values, corresponding to a period prior to dam construction in these regions. The average VCEI in the study area during this period was -0.009 . During the period from 2007 to 2014, with the advancement of large-scale dam construction projects in the Yunnan stretch, the positive expansion intensity areas gradually extended from the mid-lower to the upper regions. The average VCEI in the study area during this period was 0.006 . Between 2015 and 2020, a clear pattern of spatial clustering in VCEI emerged. The average VCEI in the study area during this period was 0.008 (county No. 41 is an outlier, so it was not considered in the calculation).

Through Figure 7g, we found that data from 2001 to 2020 elucidate a distinct spatial pattern in the basin's vegetation dynamics, closely aligned with dam construction activities. In the Yunnan stretch, there was a significant concentration of areas exhibiting high positive VCEI. These regions are identified as the most vigorously active zones for hydropower dam development, suggesting a strong link between dam construction and enhanced vegetation cover growth. Contrastingly, in the Tibetan stretch, which is characterized by its high-altitude terrain, the prevailing climatic conditions exert a more dominant influence on vegetation cover growth than hydropower dam activities. Consequently, this stretch predominantly displayed negative VCEI values, underscoring the varying impacts of environmental factors across different segments of the basin.

As shown in Figure 7d–f, from 2001 to 2006, the spatial distribution of CEI in the Tibetan stretch of the basin exhibited significant fluctuations. In the upper and mid-lower areas of the Yunnan stretch, the spatial distribution of CEI was relatively stable, with 75.6% of the counties falling within the 0.00 to 1.333 range. The average CEI in the study area during this period was 0.877 . Between 2007 and 2014, the CEI within the overall study area of the basin exhibited lower spatial resilience and significant spatial variability compared to the period before 2006. In contrast, the mid-lower Yunnan stretch was identified as high negative value area in terms of CEI. The average CEI in the study area during this period was 0.639 . From 2015 to 2020, the overall spatial distribution of CEI in the basin stabilized, with minimal disparity between high positive and low positive value areas, and overall low intensity levels across all counties. The average CEI in the study area during this period was 0.052 .

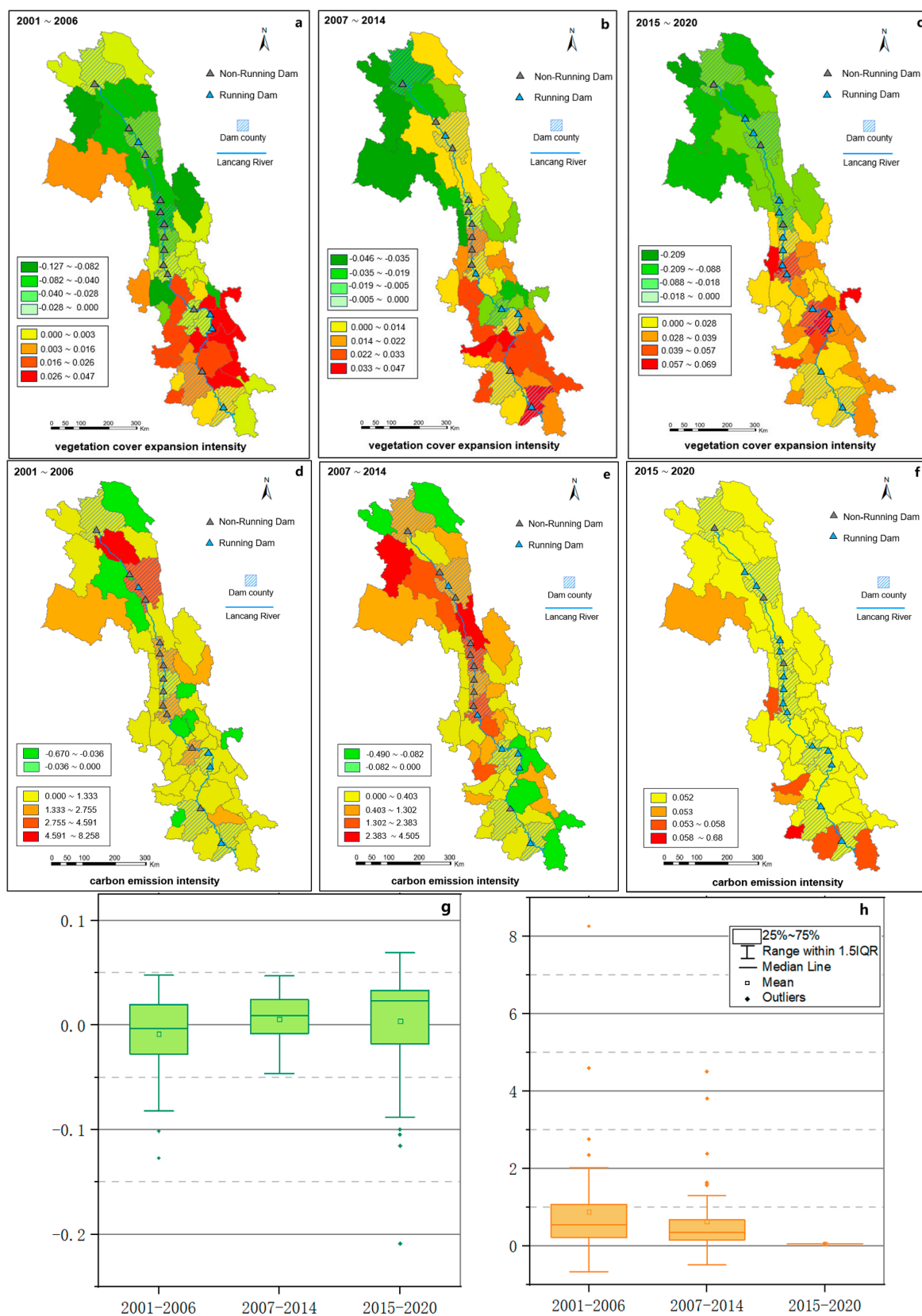


Figure 7. (a–c) The spatial distribution of VCEI across three time periods; (d–f) the spatial distribution of CEI across three time periods; (g) the trend in VCEI from 2001 to 2020; and (h) the trend in CEI from 2001 to 2020.

As shown in Figure 7h, an analysis of CEI trends in the basin from 2001 to 2020 reveals a pronounced decline aligned with the various phases of hydropower dam construction. The trend in CEI from 2001 to 2020 demonstrates a notable decrease across the three dam construction periods, with an increasingly concentrated distribution of CEI among the counties. Notably, this period witnessed a significant reconfiguration in the spatial distribution of CEI among the counties, reflecting a dynamic shift in carbon emission patterns concurrent with the dam construction timeline. The period of 2015–2020, when the majority of hydropower dams reached full operational capacity, marks the epoch of the lowest CEI in the basin. This era is characterized by a more uniform and equitable distribution of carbon emissions across the entire basin, underscoring the influential role of dam completion and operation in driving these trends.

By integrating the increased vegetation growth intensity shown in Figure 7g and the sustained increase in local population (where anthropogenic factors have been excluded from the Section 5), we can infer that local practices such as vegetation logging and stone quarrying have decreased over the years. Consequently, this suggests that the clean energy economic model, driven by hydropower and other renewable sources, has to some extent replaced the high carbon emission economic model predominantly based on vegetation logging and stone quarrying. So, the clear downward trajectory in CEI during the period of 2015–2020 highlights the positive environmental impact of dam infrastructure in facilitating a reduction in regional carbon emissions.

5. Discussion

Spanning multiple counties, our findings reveal that the average vegetation cover per square kilometer in dam counties notably exceeds that in non-dam areas, as illustrated in Figure 2. By applying data-driven time-series prediction models, we showed this substantial vegetation increase to be directly linked to dam construction. Notably, counties with hydropower dams exhibited pronounced enhancements in vegetation cover, with the NZD dam in county No. 30 showing a greater vegetative increase than that in county No. 37 (Figure 5). This disparity is partly attributed to the economic benefits to county No. 30 from hydropower-generated GDP, a sustainable and clean energy source that has replaced environmentally costly economic activities, such as tree cutting and stone mining, which were once the backbone of local economic development. So, enhanced climatic conditions and the shift towards clean energy utilization have collectively catalyzed the growth in vegetation cover in county No. 30, leading to a 7.95% higher increase in NDVI compared to county No. 37 (Figure 5). These findings underscore the key role of pivotal dam construction in both ecological restoration and the transition towards a low-carbon economy.

Our comprehensive analysis of carbon emissions in the Lancang River Basin reveals trends mirroring those observed in its changes. Figure 8a highlights that the average carbon emissions per square kilometer in dam counties are notably lower compared to those in non-dam counties. This disparity underscores the integral role of vegetation volume, economic development, and population dynamics in shaping the basin's overall carbon emissions profile. This is particularly evident in areas characterized by high expansion intensity, where significant shifts in carbon emission drivers are observed. The complex interplay of these factors highlights the multifaceted nature of carbon emission dynamics in the context of large-scale environmental and infrastructural changes. In fact, compared to numerous current studies, we have found that the impact of dam construction on vegetation is recognized as a complex interplay of both positive and negative effects. Corresponding to the scale of our research, Fu et al. (2023) reported that within sub-catchment scales there was a significant long-term increase in the average NDVI from upstream to downstream. This enhancement in vegetation health and coverage in downstream areas could be directly attributed to dam construction [43]. In our focused investigation into the effects of pivotal dams on vegetation, we observed that such dams often promote local vegetation recovery. This finding aligns with similar research conducted by Yi et al., which not only reported significant vegetation increases noted in the XW pivotal dam area between elevations of

200 and 400 m, but also highlighted that the effects of dam construction on vegetation can be both positive and negative, varying with location and altitude [44].

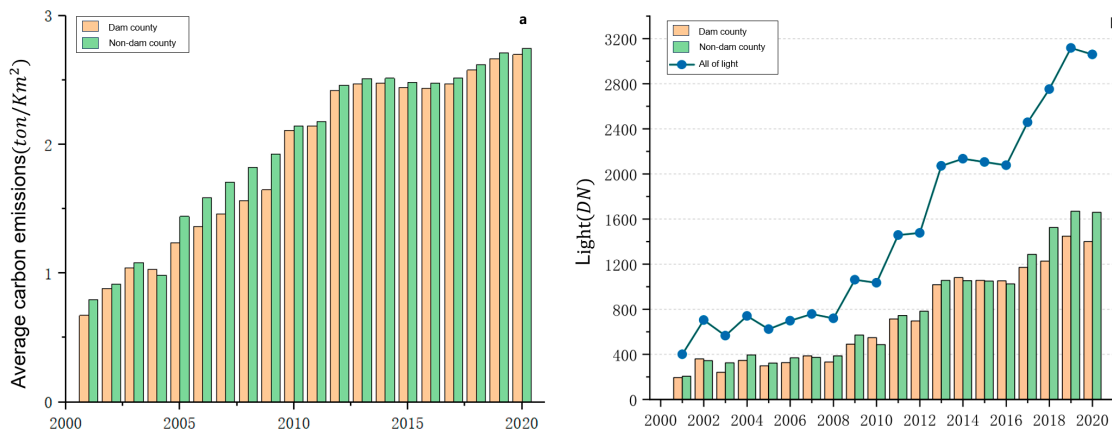


Figure 8. (a) Trends in total carbon emissions in the Lancang River Basin from 2001 to 2020. (b) Trend in light coefficient changes in the Lancang River Basin from 2001 to 2020.

Figure 8b illustrates that hydropower dam construction in the Lancang River Basin has been a catalyst for significant GDP growth, particularly in the upper Yunnan stretch from 2015 and 2020. This growth is also specifically exemplified in the study by Shi et al., which highlights the critical role of dam construction in promoting economic growth, particularly the significant impact of large dams on GDP [45]. As shown in Figure 6(b1–b3), this period saw GDP high-impact areas expand from the mid-lower to upstream regions of the basin, reflecting the economic influence of these projects over three distinct study periods from 2001 to 2020. During this time, GDP emerged as the primary driver of increased carbon emissions. From 2001 to 2014, amid evolving environmental policies and the region's relatively underdeveloped economy, economic growth was predominantly fueled by high carbon emission activities. However, the post-2015 era marked a paradigm shift. Dam construction has facilitated local development by upgrading fisheries, agriculture, and plantation industries, thereby improving the local economic revenue models [46]. Therefore, the completion of hydropower projects in the Lancang River Basin, coupled with advances in China's environmental policies, has accelerated the region's shift towards clean energy, predominantly hydropower. This shift is transforming the traditional fossil fuel-based economic system of the basin into a more sustainable, hydropower-centric, clean energy economic model.

Furthermore, the construction and operational phases of hydropower dams in the region have led to significant population influxes, particularly enhancing population mobility between 2007 and 2020, as compared to the period from 2001 to 2006. Similar to how the Belo Monte Dam in northern Brazil has increased local employment [47], the years 2007 to 2014 saw the construction of major hydropower projects in the Lancang River Basin which also created substantial employment opportunities, thereby stimulating local population growth and enhancing regional mobility. As illustrated in Figure 9a, the total population in the Lancang River Basin rose steadily from 14,941,354 in 2001 to 16,828,030 in 2020. Analysis of the data presented in Figure 9b reveals that, over these two decades, counties with dams experienced higher population growth rates than those without. This differential growth highlights the role of dam construction in influencing population dynamics. Concurrently, these population increases intensified resource demand, leading to significant carbon emissions. However, the completion of numerous hydropower dams and a transition towards cleaner energy sources from 2015 onwards contributed to a reduction in the overall carbon emissions from the population.

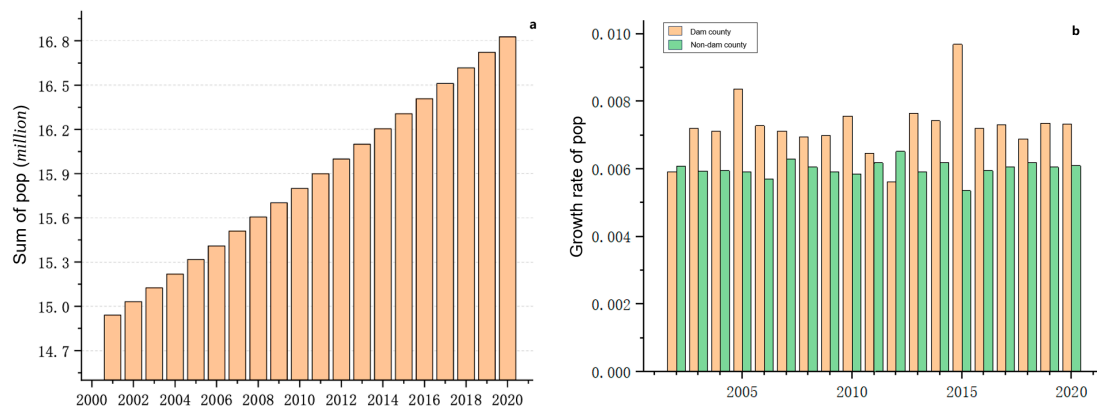


Figure 9. (a) Trends in total population in the Lancang River Basin from 2001 to 2020. (b) Trend in population growth rate in the Lancang River Basin from 2001 to 2020 (calculated based on 2001 as the growth rate benchmark).

Moreover, we found that the VCEI in the Lancang River Basin showed an increasing trend from 2001 to 2020, with spatial clustering progressively intensifying and high-intensity vegetation expansion areas gradually shifting the mid-lower Yunnan stretch. As illustrated in Figure 10, by integrating the agricultural land growth rates in the Lancang River Basin from 2001 to 2020, we observed a negative growth rate in agricultural land after 2014. However, as indicated in Figure 7g, the vegetation expansion intensity post-2014 was higher than that before 2014, coinciding with the completion and full operation of several major dams in the basin in 2014. Therefore, the increase in VCEI, calculated based on NDVI data, can be attributed not to anthropogenic factors such as the planting of crops, but to the characteristics of natural vegetation recovery. In agreement with the findings shown in Figure 10, during the dam construction period of 2011 to 2014 an increase in the rate of farmland growth was observed. The dam construction facilitated water retention in streambeds and enhanced the storage of seasonal water bodies, which spurred local agricultural development [48]. However, the rapid increase in cultivated land area often resulted in a decline in the land's agricultural carrying capacity, leading to a reduction in the total amount of farmland post-2014.

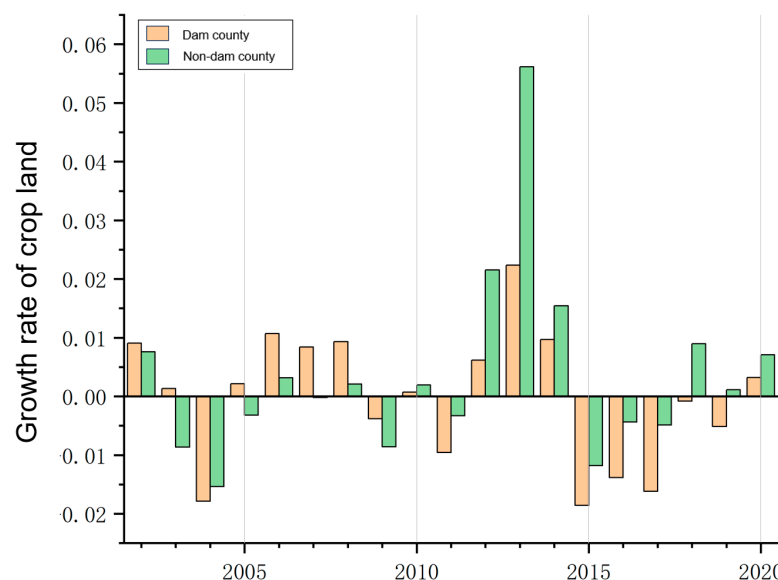


Figure 10. Trend in crop land growth rate in the Lancang River Basin from 2001 to 2020.

As shown in Figure 11, the construction of hydroelectric dams has driven the local economy, reduced the consumption of fossil fuels, and provided a large number of job opportunities for the local population, reducing the original energy dependent economic structure, jointly promoting local vegetation restoration, and increasing local carbon sinks.

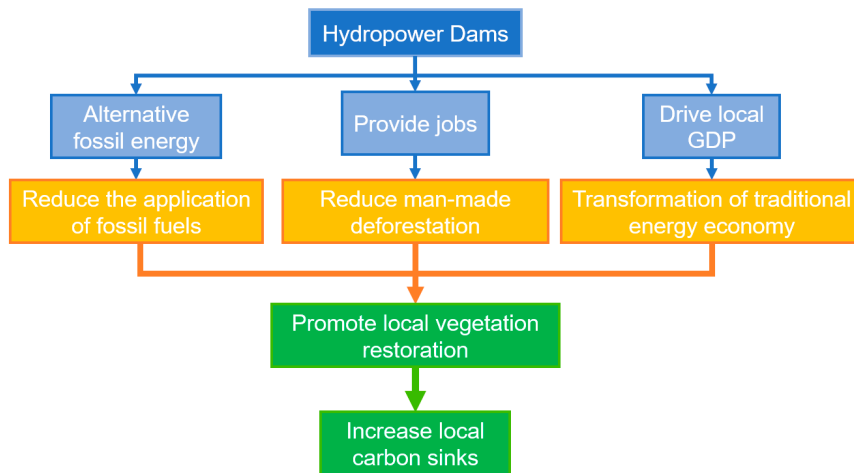


Figure 11. Hydropower dams promote local vegetation restoration and increase local carbon sinks.

6. Conclusions

Dam construction has been linked with negative environmental impacts in many previous studies [14–18], such as reduced vegetation [49], ecological invasion [50], destruction of original vegetation [51], and so on. The diminution in vegetation adversely affects the basin's carbon sequestration abilities, lowering its effectiveness as a carbon sink.

Accordingly, our research does not completely contradict earlier studies. While earlier studies have highlighted the detrimental effects of dams, such as soil erosion and habitat degradation in nearby areas due to reservoir-induced water level rises, these findings predominantly stem from investigations conducted in regions proximal to dams. Moreover, the temporal scope of these studies may have been limited, capturing only short-term impacts. In contrast, in the long term, our findings, through meticulous analysis, reveal predominantly positive impacts of hydropower dam construction on the environment. Our research underscores the importance of considering broader geographical and contextual factors when assessing the environmental implications of large-scale hydropower dam construction. So, despite stringent environmental regulations in China, the government's continued investment in hydropower dams underscores the recognition of its positive environmental contributions.

This study provides a comprehensive evaluation of the hypothesis that the construction of hydropower dams in the Lancang River Basin acts as a pivotal catalyst for enhancing vegetation restoration and advancing progress towards carbon neutrality goals. Utilizing advanced remote sensing techniques, we documented a significant increase in the local normalized difference vegetation index (NDVI) following the construction and operational onset of key hydropower dams. Specifically, during the operational phase of these dams, we observed an average NDVI increase of 16.15%, reaching a maximum of 20.12%. Over the two decades from 2001 to 2020, the commissioning of these dams has been linked to substantial alterations in ecological and carbon dynamics within the basin. Noteworthy is the shift in vegetation cover expansion intensity (VCEI) from a negative average of -0.009 to a positive mean of 0.008, reflecting a reversal from vegetation loss to significant regrowth. Concurrently, carbon emission intensity (CEI) in the vicinity of these dams has seen a dramatic reduction, plummeting from an average of 0.877 to just 0.052, indicating a major stride towards environmental sustainability. Furthermore, the increase in Global Moran's I for VCEI from 0.288 pre-2016 to 0.679 post-2015 underscores a stronger spatial autocorrelation.

tion in vegetation patterns, suggesting more cohesive and widespread ecological recovery across the basin.

Our comprehensive investigation into the basin has revealed that hydropower dams since the early 21st century have been instrumental in catalyzing vegetation restoration and development. This has notably amplified the region's carbon sequestration capacity, marking a significant stride towards environmental sustainability. Importantly, the clean energy harnessed from these hydropower dams has been pivotal in meeting local energy needs while fostering a transition from a traditional, environmentally intensive economic model to a sustainable, low-carbon economy. Our findings contribute valuable insights into the multifaceted impacts of hydropower dams, underscoring their role in ecological restoration and sustainable energy transition. From a more macro perspective, this evolution towards peak carbon and carbon neutrality aligns closely with the United Nations Sustainable Development Goals, presenting an exemplary model for global river basins considering similar infrastructural developments.

Author Contributions: Methodology, Y.L. and X.C.; Formal analysis, W.Z. and X.C.; Data curation, Y.L.; Writing—original draft, Y.L.; Writing—review & editing, Y.L. and X.C.; Supervision, X.W., G.M., W.Z. and X.C.; Project administration, X.W., G.M. and W.Z.; Funding acquisition, X.W., W.Z. and X.C. All authors have read and agreed to the published version of the manuscript.

Funding: This research was funded by the science and technology project of China HuaNeng Group, grant number HNKJ23-H1 and the National Key Research and Development Program of China, grant number 2022YFC3005505.

Data Availability Statement: All data are contained within the article.

Conflicts of Interest: Author Xiaomao Wang was employed by the company CISPDR Corporation, Changjiang Water Resources Commission of the Ministry of Water Resources. The remaining authors declare that the research was conducted in the absence of any commercial or financial relationships that could be construed as a potential conflict of interest.

References

1. Ziv, G.; Baran, E.; Nam, S.; Rodríguez-Iturbe, I.; Levin, S.A. Trading-off fish biodiversity, food security, and hydropower in the Mekong River Basin. *Proc. Natl. Acad. Sci. USA* **2012**, *109*, 5609–5614. [[CrossRef](#)] [[PubMed](#)]
2. Li, S.J.; He, D.M. Water level response to hydropower development in the upper Mekong River. *Ambio* **2008**, *37*, 170–177. [[CrossRef](#)] [[PubMed](#)]
3. Baloch, M.H.; Chauhdary, S.T.; Ishak, D.; Kaloi, G.S.; Nadeem, M.H.; Wattoo, W.A. Hybrid energy sources status of Pakistan: An optimal technical proposal to solve the power crises issues. *Energy Strategy Rev.* **2019**, *24*, 132–153. [[CrossRef](#)]
4. Yener, I.; Duman, A.; Demirarslan, K.O. The impacts of large dams on local climate in Artvin. *Fresenius Environ. Bull.* **2018**, *27*, 8468–8480.
5. Zhao, Y.Y.; Liu, S.N.; Shi, H.Y. Impacts of dams and reservoirs on local climate change: A global perspective. *Environ. Res. Lett.* **2021**, *16*, 104043. [[CrossRef](#)]
6. Fonseca, A.; Santos, J.A. The impact of a hydroelectric power plant on a regional climate in Portugal. *Atmosphere* **2021**, *12*, 1400. [[CrossRef](#)]
7. Yang, J.; Yang, Y.C.E.; Chang, J.X.; Zhang, J.R.; Yao, J. Impact of dam development and climate change on hydroecological conditions and natural hazard risk in the Mekong River Basin. *J. Hydrol.* **2019**, *579*, 124177. [[CrossRef](#)]
8. Zhong, S.; Zhu, Y.D.; Zhao, J.A.; Shen, L. A collaborative framework for hydropower development and sustainable livelihood of farmers in the Lancang-Mekong River Basin: A review with the perspective of energy-water-food nexus. *Water* **2022**, *14*, 499. [[CrossRef](#)]
9. Grumbine, R.E.; Dore, J.; Xu, J.C. Mekong hydropower: Drivers of change and governance challenges. *Front. Ecol. Environ.* **2012**, *10*, 91–98. [[CrossRef](#)]
10. Yoshida, Y.; Lee, H.S.; Trung, B.H.; Tran, H.D.; Lall, M.K.; Kakar, K.; Xuan, T.D. Impacts of mainstream hydropower dams on fisheries and agriculture in Lower Mekong Basin. *Sustainability* **2020**, *12*, 2408. [[CrossRef](#)]
11. Moran, E.F.; Lopez, M.C.; Moore, N.; Müller, N.; Hyndman, D.W. Sustainable hydropower in the 21st century. *Proc. Natl. Acad. Sci. USA* **2018**, *115*, 11891–11898. [[CrossRef](#)]
12. Renöfält, B.M.; Jansson, R.; Nilsson, C. Effects of hydropower generation and opportunities for environmental flow management in Swedish riverine ecosystems. *Freshw. Biol.* **2010**, *55*, 49–67. [[CrossRef](#)]
13. Hairan, M.H.; Jamil, N.R.; Looi, L.J.; Azmai, M.N.A. The assessment of environmental flow status in Southeast Asian Rivers: A review. *J. Clean. Prod.* **2021**, *295*, 126411. [[CrossRef](#)]

14. Fan, H.; He, D.M.; Wang, H.L. Environmental consequences of damming the mainstream Lancang-Mekong River: A review. *Earth-Sci. Rev.* **2015**, *146*, 77–91. [[CrossRef](#)]
15. Yigzaw, W.; Hossain, F. Inferring anthropogenic trends from satellite data for water-sustainability of US cities near artificial reservoirs. *Glob. Planet. Change* **2015**, *133*, 330–345. [[CrossRef](#)]
16. Liu, H.; Liu, F.; Yuan, H.M.; Zheng, L.; Zhang, Y. Assessing the relative role of climate and human activities on vegetation cover changes in the up-down stream of Danjiangkou, China. *J. Plant Ecol.* **2022**, *15*, 180–195. [[CrossRef](#)]
17. Li, J.P.; Dong, S.K.; Yang, Z.F.; Peng, M.C.; Liu, S.L.; Li, X.Y. Effects of cascade hydropower dams on the structure and distribution of riparian and upland vegetation along the middle-lower Lancang-Mekong River. *For. Ecol. Manag.* **2012**, *284*, 251–259. [[CrossRef](#)]
18. Long, S.; Zhou, S.B. Assessment on changes of ecosystem carbon storage in reservoir area due to hydroproject. *Comput. Intell. Neurosci.* **2022**, *2022*, 7511216. [[CrossRef](#)]
19. Wei, Y.M.; Chen, K.Y.; Kang, J.N.; Chen, W.M.; Zhang, X.Y.; Wang, X.Y. Policy and management of carbon peaking and carbon neutrality: A literature review. *Engineering* **2022**, *14*, 52–63. [[CrossRef](#)]
20. Liu, S.; Liu, H.M.; Chen, X.Y. Does environmental regulation promote corporate green investment? Evidence from China's new environmental protection law. *Environ. Dev. Sustain.* **2023**, *26*, 12589–12618. [[CrossRef](#)]
21. Khan, M.I.; Xu, Q.X. An assessment of environmental policy implications under the China-Pakistan Economic Corridor: A perspective of environmental laws and sustainable development. *Sustainability* **2021**, *13*, 11223. [[CrossRef](#)]
22. He, X. Dams, cropland productivity, and economic development in China. *China Econ. Rev.* **2023**, *81*, 102046. [[CrossRef](#)]
23. Fan, P.L.; Cho, M.S.; Lin, Z.H.; Ouyang, Z.T.; Qi, J.G.; Chen, J.Q.; Moran, E.F. Recently constructed hydropower dams were associated with reduced economic production, population, and greenness in nearby areas. *Proc. Natl. Acad. Sci. USA* **2022**, *119*, e2108038119. [[CrossRef](#)] [[PubMed](#)]
24. Baurzhan, S.; Jenkins, G.P.; Olasehinde-Williams, G.O. The economic performance of hydropower dams supported by the World Bank Group, 1975–2015. *Energies* **2021**, *14*, 2673. [[CrossRef](#)]
25. Gruenwald, R.; Wang, W.L.; Feng, Y. Politicization of the hydropower dams in the Lancang-Mekong Basin: A review of contemporary environmental challenges. *Energies* **2022**, *15*, 1682. [[CrossRef](#)]
26. Lang, F.S.; Liang, Y.T.; Li, S.Q.; Cheng, Z.F.; Li, G.F.; Guo, Z.J. Spatio-temporal patterns of land use and cover change in the Lancang-Mekong River Basin during 2000–2020. *Land* **2024**, *13*, 305. [[CrossRef](#)]
27. Zhang, B.Y.; Ding, W.; Xu, B.; Wang, L.F.; Li, Y.; Zhang, C. Spatial characteristics of total phosphorus loads from different sources in the Lancang River Basin. *Sci. Total Environ.* **2020**, *722*, 137863. [[CrossRef](#)]
28. Sun, Z.L.; Liu, Y.L.; Chen, H.; Zhang, J.Y.; Jin, J.L.; Bao, Z.X.; Wang, G.; Tang, L. Evaluation of future climatology and its uncertainty under SSP scenarios based on a bias processing procedure: A case study of the Lancang-Mekong River Basin. *Atmos. Res.* **2024**, *298*, 107134. [[CrossRef](#)]
29. Ruigar, H.; Golian, S. Prediction of precipitation in Golestan dam watershed using climate signals. *Theor. Appl. Climatol.* **2016**, *123*, 671–682. [[CrossRef](#)]
30. Abu-Afifeh, Q.; Rahbeh, M.; Al-Afeshat, A.; Al-Omari, S.; Qutishat, T.A.; Brezat, A.; Alkayed, A. Dam sustainability's interdependency with climate change and dam failure drivers. *Sustainability* **2023**, *15*, 16239. [[CrossRef](#)]
31. Ren, Q.S.; Li, C.X.; Yang, W.H.; Song, H.; Ma, P.; Wang, C.Y.; Schneider, R.L.; Morreale, S.J. Revegetation of the riparian zone of the Three Gorges Dam Reservoir leads to increased soil bacterial diversity. *Environ. Sci. Pollut. Res.* **2018**, *25*, 23748–23763. [[CrossRef](#)]
32. Chen, Z.Q.; Yu, B.L.; Yang, C.S.; Zhou, Y.Y.; Yao, S.J.; Qian, X.J.; Wang, C.; Wu, B.; Wu, J. An extended time series (2000–2018) of global NPP-VIIRS-like nighttime light data from a cross-sensor calibration. *Earth Syst. Sci. Data* **2021**, *13*, 889–906. [[CrossRef](#)]
33. Bickenbach, F.; Bode, E.; Nunnenkamp, P.; Söder, M. Night lights and regional GDP. *Rev. World Econ.* **2016**, *152*, 425–447. [[CrossRef](#)]
34. Yang, J.; Huang, X. The 30 m annual land cover dataset and its dynamics in China from 1990 to 2019. *Earth Syst. Sci. Data* **2021**, *13*, 3907–3925. [[CrossRef](#)]
35. Karingula, S.R.; Ramanan, N.; Tahmasbi, R.; Amjadi, M.; Jung, D.; Si, R.; Thimmisetty, C.; Polania, L.F.; Sayer, M.; Taylor, J. Boosted embeddings for time-series forecasting. In Proceedings of the 7th International Conference on Machine Learning 2021, Optimization, and Data Science (LOD)/1st Symposium on Artificial Intelligence and Neuroscience (ACAIN), Electr Network, Grasmere, UK, 4–8 October 2021; pp. 1–14.
36. Liu, S.W.; Jiao, Y.; Sun, Q.T.; Jiang, J.H. Estimation of sea level change in the South China Sea from satellite altimetry data. *Sci. Program.* **2021**, *2021*, 6618135. [[CrossRef](#)]
37. Guo, L.; Fang, W.G.; Zhao, Q.H.; Wang, X. The hybrid PROPHET-SVR approach for forecasting product time series demand with seasonality. *Comput. Ind. Eng.* **2021**, *161*, 107598. [[CrossRef](#)]
38. He, J.; Yang, J. Spatial-temporal characteristics and influencing factors of land-use carbon emissions: An empirical analysis based on the GTWR model. *Land* **2023**, *12*, 1506. [[CrossRef](#)]
39. Fotheringham, A.S.; Crespo, R.; Yao, J. Geographical and temporal weighted regression (GTWR). *Geogr. Anal.* **2015**, *47*, 431–452. [[CrossRef](#)]
40. Mohammadnazar, A.; Mahdinia, I.; Ahmad, N.; Khattak, A.J.; Liu, J. Understanding how relationships between crash frequency and correlates vary for multilane rural highways: Estimating geographically and temporally weighted regression models. *Accid. Anal. Prev.* **2021**, *157*, 106146. [[CrossRef](#)]
41. Chen, Y.G. New approaches for calculating Moran's index of spatial autocorrelation. *PLoS ONE* **2013**, *8*, e68336. [[CrossRef](#)]

42. Peng, S.P.; Shi, G.Q.; Zhang, R.L. Social stability risk assessment: Status, trends and prospects—A case of land acquisition and resettlement in the hydropower sector. *Impact Assess. Proj. Apprais.* **2021**, *39*, 379–395. [[CrossRef](#)]
43. Fu, J.J.; Wang, W.; Hunter, P.D.; Li, W.; Sun, J.Y. Trends in normalized difference vegetation index time series in differently regulated cascade reservoirs in Wujiang catchment, China. *Ecol. Indic.* **2023**, *146*, 109831. [[CrossRef](#)]
44. Yi, Y.J.; Zhou, Y.; Song, J.; Zhang, S.H.; Cai, Y.P.; Yang, W.; Yang, Z. The effects of cascade dam construction and operation on riparian vegetation. *Adv. Water Resour.* **2019**, *131*, 103206. [[CrossRef](#)]
45. Shi, H.Y.; Chen, J.; Liu, S.N.; Sivakumar, B. The Role of Large Dams in Promoting Economic Development under the Pressure of Population Growth. *Sustainability* **2019**, *11*, 2965. [[CrossRef](#)]
46. Alrajoula, M.T.; Al Zayed, I.S.; Elagib, N.A.; Hamdi, M.R. Hydrological, socio-economic and reservoir alterations of Er Roseires Dam in Sudan. *Sci. Total Environ.* **2016**, *566*, 938–948. [[CrossRef](#)]
47. Bro, A.S.; Moran, E.; Calvi, M.F. Market Participation in the Age of Big Dams: The Belo Monte Hydroelectric Dam and Its Impact on Rural Agrarian Households. *Sustainability* **2018**, *10*, 1592. [[CrossRef](#)]
48. Almalki, R.; Khaki, M.; Saco, P.M.; Rodriguez, J.F. The impact of dam construction on downstream vegetation area in dry areas using satellite remote sensing: A case study. *Remote Sens.* **2023**, *15*, 5252. [[CrossRef](#)]
49. Uddin, F.M.J.; Asaeda, T.; Rashid, M.H. Large-scale changes of forestation in river channel below the dams in southern African rivers: Assessment using Google Earth images. *Pol. J. Ecol.* **2014**, *62*, 607–623. [[CrossRef](#)]
50. Illeperuma, N.D.; Dixon, M.D.; Elliott, C.M.; Magnuson, K.I.; Withanage, M.H.H.; Vogelmann, J.E. Spatiotemporal patterns and environmental drivers of eastern redcedar (*Juniperus virginiana*) abundance along the Missouri River, USA. *Landscape Ecol.* **2023**, *38*, 1677–1695. [[CrossRef](#)]
51. Yan, D.H.; Wang, H.; Li, H.H.; Wang, G.; Qin, T.L.; Wang, D.Y.; Wang, L.H. Quantitative analysis on the environmental impact of large-scale water transfer project on water resource area in a changing environment. *Hydrol. Earth Syst. Sci.* **2012**, *16*, 2685–2702. [[CrossRef](#)]

Disclaimer/Publisher's Note: The statements, opinions and data contained in all publications are solely those of the individual author(s) and contributor(s) and not of MDPI and/or the editor(s). MDPI and/or the editor(s) disclaim responsibility for any injury to people or property resulting from any ideas, methods, instructions or products referred to in the content.